TWENTYFIFTH EUROPEAN ROTORCERAFT FORUM

Paper n° B2

IMPULSIVE NOISE CALCULATION USING MOVING OVERLAPPED GRID METHOD / KIRCHHOFF METHOD

By

Shigeru Saito and Takashi Aoyama
National Aerospace Laboratory, Japan

Akio Ochi and Natsuki Kondo
Advanced technology Institute of Commuter Helicopter

Ayumu Yamaguchi
Tokai University

SEPTEMBER 14-16, 1999
ROME
ITALY

ASSOCIAZIONE INDUSTRIE PER L'AEROSPAZIO, I SISTEMI E LA DIFES A
ASSOCIZIONE ITALIANA DI AERONAUTICA ED ASTRONAUTICA

Impulsive Noise Calculation using Moving Overlapped Grid Method / Kirchhoff Method

Shigeru Saito and Takashi Aoyama
National Aerospace Laboratory
7-44-1, Jindaijihigashimachi, Chofu, Tokyo 182-8522

Akio Ochi and Natsuki Kondo
Advanced Technology Institute of Commuter Helicopter
2 Kawasaki-Cho, Kakamigahara, Gifu, 504-8710

Ayumu Yamaguchi
Tokai University
1117 Kitakaname Hiratsuka Kanagawa 259-1292

Abstract

The predictions of helicopter high-speed impulsive (HSI) noise are preformed using a combined method of an unsteady Euler code with an aeroacoustic code based on the Kirchhoff formulations. A moving overlapped grid method (MOGM) is employed in the Euler code. Three types of grids, blade grid, inner and outer background grids are used. The calculated waveform of HSI noise showed good correlation with experiment. In comparison with acoustic codes of Kirchhoff and Ffowcs Williams and Hawkings formulation, acoustic waveform calculated by means of FW-H formulation showed underpredicted noise pressure level. This combined method is applied to predict a HSI noise of the Advanced Technology Institute of Commuter Helicopter (ATIC) blade (AT1). The calculated results showed that AT1 blade has low HSI noise characteristics.

Nomenclature

c	: chord length
Cp	: pressure coefficient (normalized by local dynamic pressure)
M_{tip}	: tip Mach number (hover)
M_∞	: free stream Mach number
r	: span-wise station
R	: rotor radius
T	: period
α_i	: shaft tilt angle
β_{av}	: average flapping angle
β_t	: blade twist angle
θ_0	: collective pitch angle
θ_{1c}	: lateral cyclic angle
θ_{1s}	: longitudinal cyclic angle
μ	: advance ratio, M_∞ / M_{tip}
ω	: vorticity vector
Ω	: rotor rotational speed
$\|\omega\|$	: vorticity magnitude
ψ	: azimuthal angle

1. Introduction

In the last twenty years, much effort has been devoted to helicopter rotor noise analysis on order to reduce the acoustic nuisance. The impulsive noise generated from the main rotor of a helicopter is a very typical and annoying problem for helicopters. This is the main issue for the future quiet helicopters because it must be mainly used

inside or near the densely populated areas. This type of noise occurs in two cases. One of them is blade-vortex interaction (BVI) noise, which is caused by the sudden change of blade loads during the interaction of blades with previously shed tip vortices. In general, the interaction occur in descent flight conditions, especially during approach and landing. The second type of impulsive noise is high-speed impulsive (HSI) noise, which is caused by shock wave generated on the blade surface of the advancing side in high-speed forward flight. This noise propagates toward in-plane observer positions. The intensity of the HSI noise is affected by the occurrence of the delocalization, which happens when the supersonic region on the blade surface connects with the sonic cylinder, where the undisturbed flow appears to is strong disturbance caused by the wave to propagate toward the far field.

There are so many papers, which deals with the helicopter noise. In rotor noise analysis, the method solving the Ffowcs Williams and Hawkings (FW-H) formulation[1] has often used. It is a generalized of Lighthill's[2] Acoustic Analogy (LAA) in the presence of moving surfaces. Although this method shows the good capability of predicting the noise from a subsonic rotor[3,4,5], it does not succeed in predicting the HSI noise generating by a rotor in transonic forward flight configuration. Indeed, the evaluation of the quadrupole term in the FW-H formulation is very difficult[6,7,8,9]. Another method was used to successfully predict the HSI noise an about three rotor radii for non-lifting rotors in Hover. However, it remains very complex to predict the far-field noise because of the difficulty to maintain an adequate grid resolution in the far field. For forward flight applications, a direct computation seems to be unrealistic because of excessive CPU cost. A combined CFD method with the Kirchhoff formulation[10,11] can also be used to analyze the HSI noise problem in hover[12,13] and in forward flight[14,15,16,17].

At National Aerospace Laboratory, the rotorcraft special research has been started since 1996. At the same time, the collaborative research cooperation initiated between NAL and ATIC for the purpose of the development of the rotorcraft noise analysis code, especially impulsive noise of helicopter. At first stage, as the aerodynamic code, steady and unsteady Euler codes[18,19] have been used in order to simulate the flowfield around a blade and then it has been combined with the acoustic code based on Kirchohoff formulation[3]. This combined method has been successfully applied to the investigation of HSI noise in the case of hovering flight[20,21,22] and showed good correlation with experimental data. Using the same code, this method has been compared with ONERA's aeroacoustic code under the collaborative research cooperation. It was shown that our code has same capability to predict the HSI noise go a helicopter as one of ONERA's code[23]. Besides the combined method with the unsteady Euler code and the Ffowcs-Williams and Hawkings (FW-H) formulation[4] has been developed under the collaborative research cooperation with ATIC. The trajectory of the tip vortices were calculated by CAMRAD Ⅱ. In this combined method, the effective angles of attack of a blade were transported to the CFD calculation[24]. The calculated BVI noise used this code was compared with the experimental data at DNW test conducted by ATIC[25]. It was shown that this combined method overpredicted the noise level and presented the different directivity of the overall noise for the test data. This discrepancy comes from the trajectory of the tip vortices shed from the previous blade tip. CAMRAD Ⅱ can supply the tip vortex trajectory using the vortex theory. However it seems to be less accurate to predict the tip vortex trajectory. On the contrary, the moving overlapped grid method (MOGM) has capability to precisely predict the trajectory of the tip vortex without any assumption such as vortex core size, roll-up position etc. From this point of view, the moving overlapped grid method was developed under the collaborative research cooperation between NAL and ATIC and applied to the BVI noise prediction combined with FW-H formulation[26,27,28]. This method needs huge number of grid points and huge storage of pressure data. The numerical Wind Tunnel (NWT) of NAL was used in order to calculate the flowfield around a helicopter rotor.

In this paper, the MOGM is applied to simulate the flowfield around a rotor blade in forward flight. This method is coupled with the rotating Kirchhoff formulation in order to predict HSI noise at the observer points. A rotating Kirchhoff formulation is used and it allows the Kirchhoff surface to rotate with the blade. The predicted noise waveforms are compared with experimental data and

also the directivity of HSI noise is investigated.

2. Numerical method

The procedure of HSI noise prediction consists of two phases. The first phase is a CFD computation of the rotor aerodynamics. The second one is an acoustic computation to obtain far field acoustic data using the rotating Kirchhoff surface pressure computed in the first phase.

2.1 Governing Equations

The governing equations of the aerodynamic computation are the unsteady 3-dimensional Euler equations. The inertial force terms by the rotation are included in the calculation of the blade grid[18].

2.2 Grid system

A moving overlapped grid approach is employed to treat rotating rotor blades. The grid system for a 5-bladed configuration used in our previous study is sketched in Fig. 1. The blade grid rotates in the Cartesian background grid.

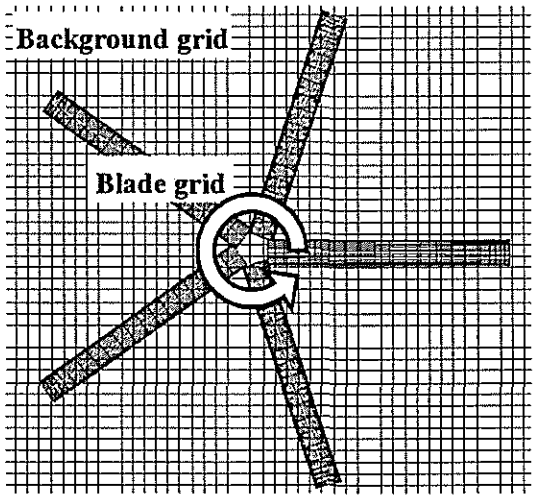

Fig. 1 Blade grids and background grid for 5-bladed rotor computation.

In this study, a new grid topology is employed to concentrate grid points near the rotor disk. The Cartesian background grid is divided into the two parts as shown in Figs. 2 and 3. One is the inner background grid and the other is the outer background grid. The inner background grid is placed around the rotor disk. The outer background grid covers whole computation region and has sparse grid density. The flow data are exchanged between inner and outer background grids. The size of the two background grids for forward flight calculation is shown in Fig. 4. Huge number of grid points is distributed to the inner background grid to achieve higher resolution, because the density of grid directly affects the strength of numerical viscosity.

The blade grid wraps rotor blade using BFC and moves with the blade motions, such as rotation, flapping, feathering, and lagging. It is provided for each blade in multi-bladed computations as shown in Fig. 3. The flow data are exchanged between the blade grids and the inner background grid at the outer boundary of the blade grids. The blade grid is generated by an algebraic formulation and has an O-H type topology. The number of grid points in span-wise direction is considerably increased to match the grid density of the blade grid with that of the inner background grid. The size of the blade grid in normal direction is nearly twice to the chord length as shown in Fig. 5.

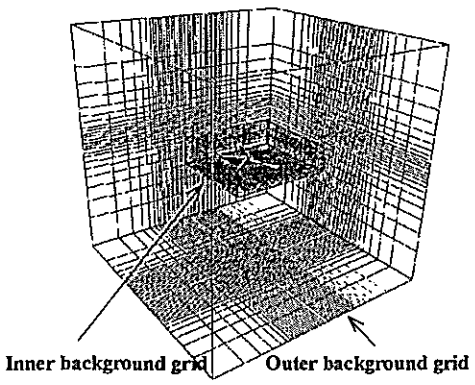

Fig.2 Blade grids, inner background grid, and outer background grid.

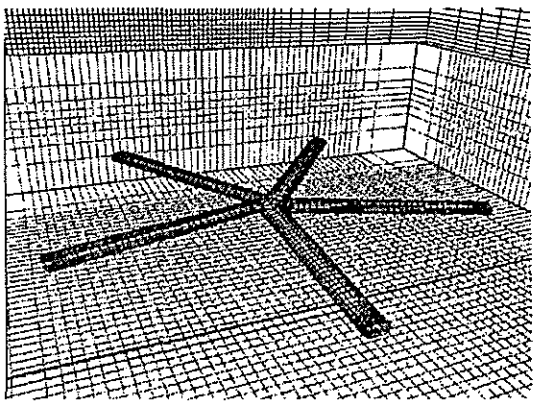

Fig. 3 Blade grids and background grids.

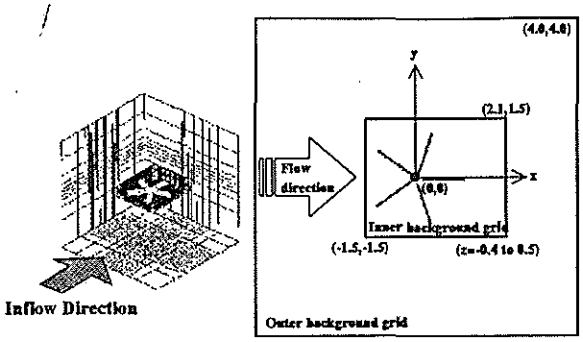

Fig.4 Size of computation regions of inner and outer background grids.

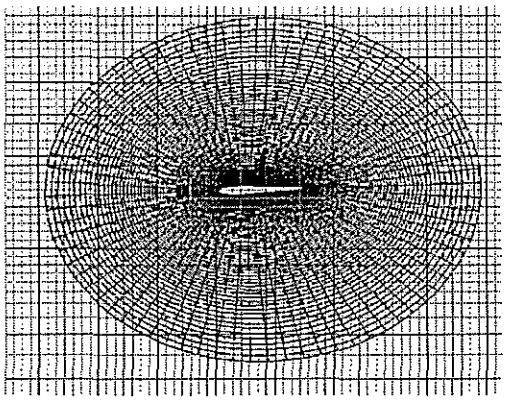

Fig.5 Cross section of blade grid and inner background grid.

Table 1 shows the numbers of grid points. The grid spacing of the inner background grid correspond to $0.0945c$ (OLS blade) and $0.189c$ (Baseline and AT1 blade); where c is the chord length.

Table 1. Grid specifications.

	OLS blade	B.L. and AT1
Inner background grid	(x × y × z) 290 x 230 x 50 = 3,335,000	
Outer background grid	(x × y × z) 83 x 79 x 49 = 321,293	
Blade grid	(chord x normal x span) x blade	
	(77x80x95)x2 = 1,170,400	(79x60x155)x5 =3,673,500
Total	4,826,693 points	7,329,793 points
Grid spacing of inner background grid in rotor disk	0.0945c (= 0.006R)	0.189c (=0.0104R)

2.3 Numerical method for Cartesian background grid

A high accuracy explicit scheme is utilized in the background Cartesian grid. The compact TVD scheme is employed for spatial discretization[29]. MUSCL cell interface value is modified to achieve 4th-order accuracy. Simple High-resolution Upwind Scheme (SHUS) [30] is employed to obtain numerical flux. SHUS is one of the Advection Upstream Splitting Method (AUSM) type approximate Riemann solvers and has small numerical diffusion. The time integration is carried out by an explicit method. The four stage Runge-Kutta method is used for the present calculation. The free stream condition is applied for the outer boundary of the outer background grid.

2.4 Numerical method for blade grid

The numerical method for the blade grid calculation is an implicit finite-difference scheme[18]. The transformed equations are written as

$$\frac{\partial Q}{\partial t}+\frac{\partial F_i}{\partial \xi_i}+H=0, \tag{1}$$

where

$$Q=J^{-1}\begin{pmatrix}\rho\\ \rho u_1\\ \rho u_2\\ \rho u_3\\ e\end{pmatrix},\quad F_i=J^{-1}\begin{pmatrix}\rho U_i\\ \rho u_1 U_i+\xi_{i,1p}\\ \rho u_2 U_i+\xi_{i,2p}\\ \rho u_3 U_i+\xi_{i,3p}\\ (e+p)U_i+\xi_{i,tp}\end{pmatrix},\quad H=J^{-1}\begin{pmatrix}0\\ -\rho\Omega u_2\\ \rho\Omega u_1\\ 0\\ 0\end{pmatrix}. \tag{2}$$

In these equations,

$$\begin{aligned}&(\ )_{,t}=\frac{\partial}{\partial t},\\ &(\ )_{,j}=\frac{\partial}{\partial x_j},\\ &(x_1,x_2,x_3)=(x,y,z),\\ &(\xi_1,\xi_2,\xi_3)=(\xi,\eta,\zeta),\\ &(u_1,u_2,u_3)=(u,v,w),\\ &(U_1,U_2,U_3)=(U,V,W).\end{aligned} \tag{3}$$

The quantity ρ is the density, u, v, and w are the velocity components in the cartesian coordinate system, and U, V, W are the contravariant components of the velocity. The quantity Ω is the angular velocity of the blade rotation, and p is the pressure which is represented as

$$p=(\gamma-1)\left(e-\frac{1}{2}\rho u_i^2\right) \tag{4}$$

where γ is the ratio of specific heat and e is the total

energy per unit volume. The quantity J is the Jacobian of the transformation between cartesian and computational coordinate.

The numerical method to solve the governing equations is an implicit finite-different scheme. The Euler equations are discretized in the conventional delta form using the Euler backward time differencing. A diagonalized ADI method based on an upwind flux-split technique is used for the implicit left-hand-side regarding the spatial differencing. In addition, a higher-order upwind scheme based on TVD is applied for the inviscid terms of the explicit right-hand-side. Each ADI operator is decomposed into the product of lower and upper bidiagonal matrices by using diagonally dominant factorization. In addition, an upwind scheme based on TVD by Chakravarthy and Osher is applied for the inviscid terms of the explicit right-hand-side. Each operator is decomposed into the product of lower and upper bi-diagonal matrices by using diagonally dominant factorization. The accuracy of this solver in space and in time is 2nd-order and 1st-order, respectively. In order to obtain the unsteady solution in forward flight conditions, the Newton iterative method is also used. In order to reduce the residual at each time-step, six iterations are used.

The typical dividing number along the azimuthal direction is about 10,000 per revolution for the OLS and other blades. It corresponds azimuth angles about 0.036°. The unsteady calculation is impulsively started from the azimuth angle of 0°.

2.5 Interpolation of flow data

The search and interpolation to exchange flow data, $Q=(\rho, \rho u, \rho v, \rho w, e)^t$, between the grids are executed in each time step because the blade grid rotates with the rotor blade in the background grids. The computation time spent for search and interpolation is one of the disadvantages of the moving overlapped grid approach. In our computation, this problem is severe because a vector and parallel computer is used. Therefore, a new algorithm using tri-liner interpolation is developed and it is vectorized and paralellized[31]. The typical calculation time for the interpolation is about 20% of all calculation time in the parallel computation of 5-bladed rotor case.

2.6 Treatment of blade motion

The dynamic blade motions such as flapping, feathering, and lagging are defined by the input data. This code accepts azimuth-wise data or 1st harmonic function data obtained by measurements or other codes (e.g. CAMRAD). In the present calculation, the collective pitch and cyclic pitch angles by the wind tunnel experiment are used. The preset coning angles are only used as the flapping motion. The inertial forces by these dynamic motions have not considered yet in the present flow solver.

2.7 Noise analysis

The pressure distribution on the blade surface calculated by the CFD code is stored every 1.0° at the range from 70° to 130° in the azimuth-wise direction as the input data. In the other range of azimuthwise direction, the pressure distributions are stored at every 10°. The aeroacoustic code is based on the extended Kirchhoff formulation based on the Farassat and Myers[32].

The acoustic pressure p, which is the function of an observer position x and an observer time t, satisfies the wave equation as follows:

$$\left(\frac{1}{c^2}\frac{\bar{\partial}^2 p}{\partial t^2}-\bar{\nabla}^2 p\right)\cdot H(f) = -\left(\hat{p}_n+\frac{1}{c}M_n\hat{p}_t\right)\delta(f)-\frac{1}{c}\frac{\bar{\partial}}{\partial t}\{M_n\hat{p}\delta(f)\}-\bar{\nabla}\cdot\{\hat{p}n\delta(f)\} \tag{5}$$

where $H(f)$ is the Heaviside function and $\delta(f)$ is the Dirac delta function. The quantity c is the speed of sound. The Kirchhoff surface S in which all the acoustic sources are enclosed is described by $f=0$ such that $f>0$ defines the exterior of S. The bar over the operator symbol denotes operators involving generalized derivatives[33]. The vector n and $M_n, \hat{p}, \hat{p}_n$, and $\hat{p}_t$ in equation (5) are described as follows:

$$\begin{aligned} n &= \nabla f, \\ M_n &= \frac{1}{c}\frac{\partial f}{\partial t}, \\ \hat{p} &= \lim_{f\to+0} p(x,t), \\ \hat{p}_n &= \nabla\hat{p}\cdot\nabla f, \\ \hat{p}_t &= \frac{\partial\hat{p}}{\partial t}. \end{aligned} \tag{6}$$

By using the Green function in unbounded space, equation (5) gives

$$p(x,t)\cdot H(f)=$$

$$\int_{-\infty}^{t} d\tau \int G^0\left[-\left(\hat{p}_n+\frac{1}{c}M_n\hat{p}_t\right)\delta(f)-\frac{1}{c}\frac{\partial}{\partial t}\left[M_n\hat{p}\delta(f)\right]-\nabla\cdot\left[\hat{p}n\delta(f)\right]\right]dy, \tag{7}$$

where

$$G^0(y,\tau\,|\,x,t)=\frac{1}{4\pi r}\delta(g), \tag{8}$$

and

$$g=\tau-t+\frac{r}{c}. \tag{9}$$

In equation (7), the vector y is a source position, τ is a source time. In equation (9), r is the distance between a source and an observer position. By performing the integration on the influential surface in equation (7), the following is obtained.

$$4\pi p(x,t)\cdot H(f)=$$

$$-\int\frac{\hat{p}_n+M_n\hat{p}_t/c}{r\Lambda}d\Sigma+\int\frac{\hat{p}\cos\theta}{r^2\Lambda}d\Sigma+\frac{1}{c}\frac{\partial}{\partial t}\int\frac{(\cos\theta-M_n)\hat{p}}{r\Lambda}d\Sigma, \tag{10}$$

where

$$\Lambda=\sqrt{1+M_n-2M_n\cos\theta} \tag{11}$$

In equation (10), Σ is the influential surface generated by all Γ-curves as the source time τ varies $-\infty$ to t for the fixed observer position x and time t, where the Γ-curve is the intersection of body and sphere $g=0$. The function g is defined by equation (9) and $g=0$ shows the sphere on

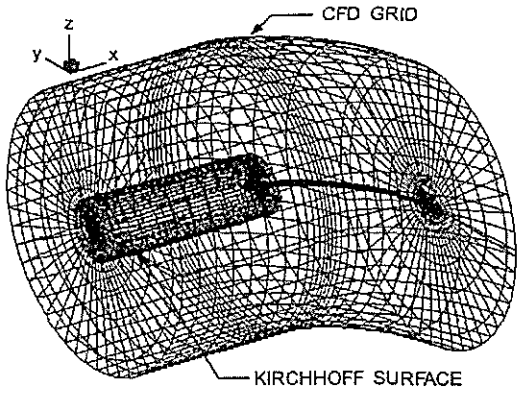

Fig.6 Euler and Kirchhoff grids for noise analysis.

which the acoustic pressure transmits in the space. The quantity θ is the angle between n and r.

The Kirchhoff surface used here is selected to correspond with the finite difference grid used in the Euler calculation. The top view of the surface is shown as the hatched region in Fig. 6. The size of the surface was determined by a preliminary size sensitivity study mentioned later.

2.9 Calculation conditions

The dimension of the calculated rotor and the operating conditions are summarized in Tables 2 and 3. OLS blade[34] and baseline and AT1 blade are selected in this calculation. Same conditions are used for the baseline and AT1 blades in the ATIC model rotor.

Table 2. Dimensions of blades.

	OLS blade	Baseline blade	AT1 blade
Number of blades	2	5	5
Rotor radius, R (m)	0.958	2.0	2.0
Chord length, c (m)	0.104	0.11	0.11
Blade twist, β_1 (deg)	-10.0°	-8.0°	-8.0°
Aspect ratio	9.0	18.0	18.0
Airfoil	BHT540mod	NACA23012mod	AK100D/AK80A

Table 3. Operating conditions.

	OLS blade	Baseline blade	AT1 blade
Shaft tilt angle, α_s	3.25°(aft)	5.00°(aft)	5.00°(aft)
Collective pitch angle, θ_0	7.66°	8.00°	8.00°
Lateral cyclic pitch angle, θ_{1c}	-1.00°	-2.45°	-2.45°
Longitudinal cyclic pitch angle, θ_{1s}	4.47°	6.68°	6.68°
Flapping angle (averaged), β_{av}	0.5°	2.894°	2.894°
Tip Mach number, M_{tip}	0.664	0.6176	0.6176
Advance ratio, μ	0.258	0.34	0.34

3./Results and Discussion

Numerical computations are performed by the present method for three types of blade, i.e. OLS blade, baseline blade with NACA 23012 mod wing section, and AT1 blade by ATIC. The calculated pressure on the Kirchhoff surface is used as the input data for aeroacoustic code based on Kichhoff formulation.

These calculations are impulsively started from a free stream condition. The computation is carried out on Numerical Wind Tunnel (NWT) in NAL to perform large scale and accurate computations. NWT is a vector parallel super computer consists of 166 processing elements (PE). Each processing element has a vector processor with 1.7 G flops peak performance. The CPU time is about 40 hours per revolution using 16 PEs for OLS blade and 60 hours using 18 PEs for the baseline blade with NACA23012mod wing section and AT1 blade. The periodic solution is obtained after 3 revolutions. The required memory sizes are about 450MB and 620MB for the OLS and the baseline and AT1 blade cases, respectively.

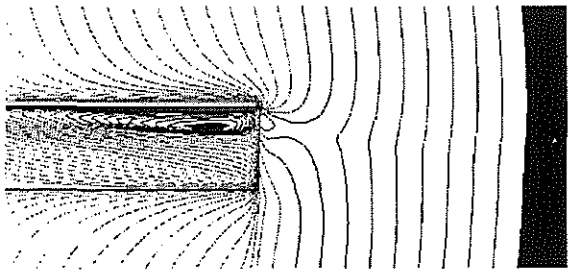

(a) OLS blade

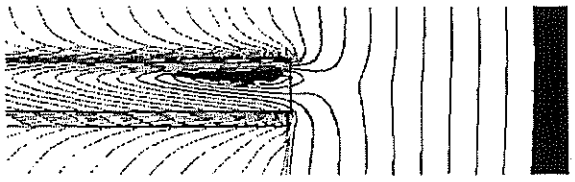

(b) Rectangular blade

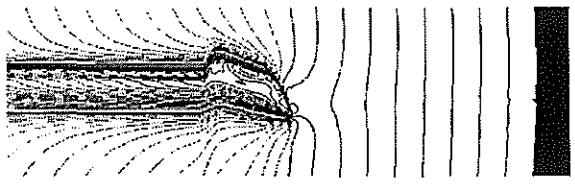

(c) AT1 blade

Fig.7 Velocity distribution around a blade

3.1 Aerodynamics

Figure 7 shows velocity contours around a blade for three blades. The tip mach number for each blade are 0.664 and 0.618 for OLS blade and baseline and AT1, respectively. In this condition, the delocalization does not appear at the tip region. However near the tip region on a blade, supersonic pocket exists for all blades. Calculated Cp distributions apparently show the existence of the weak shock. The supersonic pocket for the AT1 blade is the smallest compared with other blades. Fig.8 shows load distributions for each rotor. The thrust coefficient has been compared between calculated results and experiment. Calculated thrust coefficient well coincident with experimental data. However thrust coefficient for OLS rotor shows lower value about 9% than experiment because of the rearrangement of the control inputs. In the calculation, the flapping angle of just preconing angle only is involved in the calculation. Therefore the longitudinal cyclic pitch angle was subtracted by the longitudinal flapping angle. Fig.9 shows the iso-surface of vorticity magnitude in the inner background grid, its magnitude is $\| \omega \| = 0.7$ for each rotor. From this figure, the tip vortices are well captured in this calculation.

3.2 Aeroacoustics

Fig.10 shows the microphone positions in the experiment. The sound pressure level (SPL) were calculated foe the three rotor blades. At the first stage of the calculation, the sensitivity of the Kirchhoff Surface on the SPL is investigated. Fig.11 and Fig.12 show the sensitivity on the SPL for the OLS blade. In the normal direction to a blade, $2.02c$ (upper or lower surface direction of a blade) or $2.26c$ (leading edge or trailing edge direction of a blade) is best fitting to the experimental data. For further distance from a blade, the calculated results show the worse SPL compared with the data. On the other hand, the case of $1.35R$ in the spanwise direction shows best fitting with data. From this parametric study, the distance from a blade was decided as follows: normal direction is $20.2c$ and spanwise direction is $1.35R$. This definition of a Kirchhoff surface is also used in the calculation for baseline and AT1 blades.

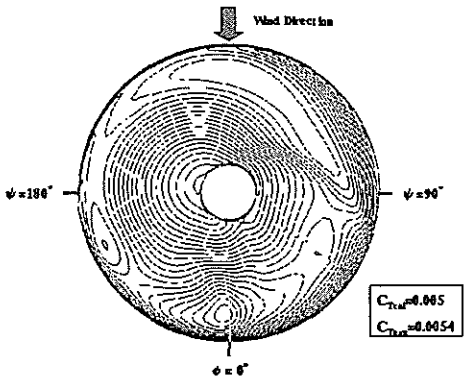

(a) OLS blade

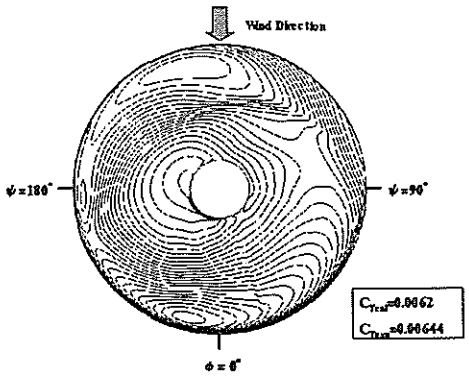

(b) Baseline blade

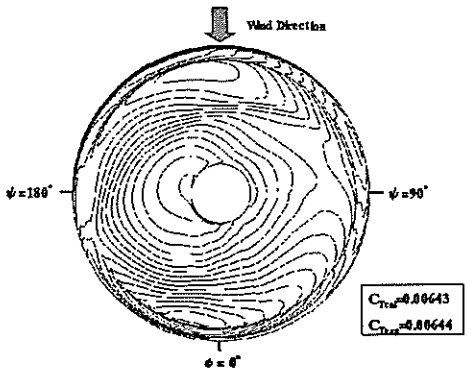

(c) AT1 blade

Fig.8 Load distributions on each rotor.

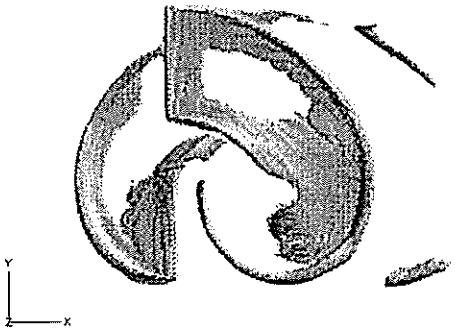

(a) OLS blade

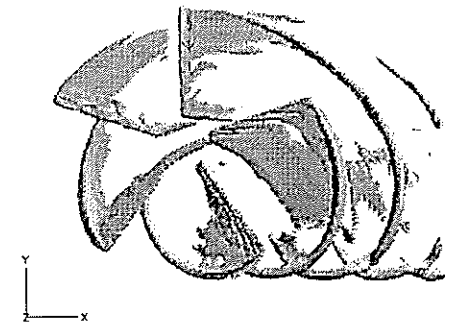

(b) Baseline blade

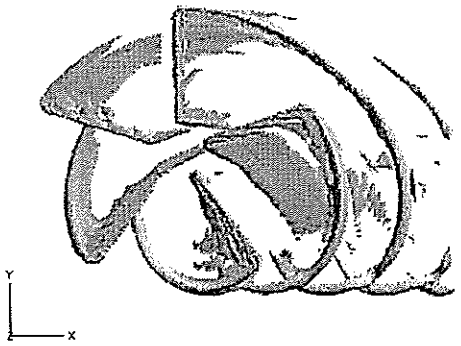

(c) AT1 blade

Fig.9 Visualized vortices by iso-surface of vorticity magnitude for each blade.($\| \omega \| = 0.7$)

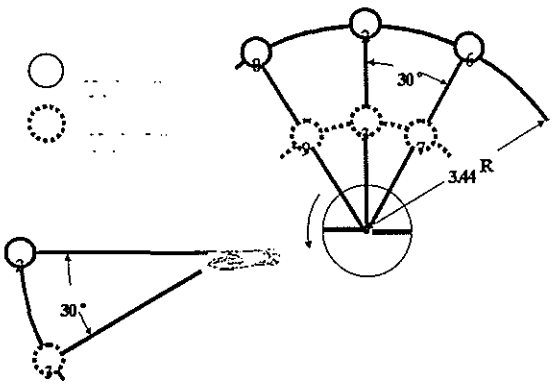

Fig. 10 Microphone positions in the experiment[34].

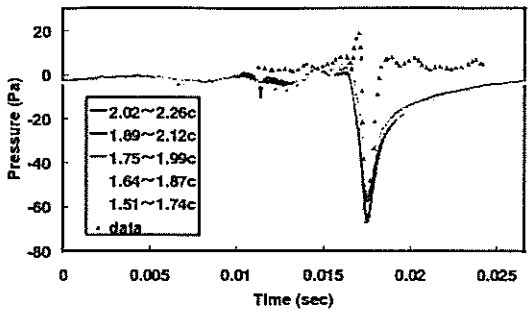

Fig.11 Sensitivity of the Kirchhoff surface on the SPL in the normal direction to a blade for OLS blade.

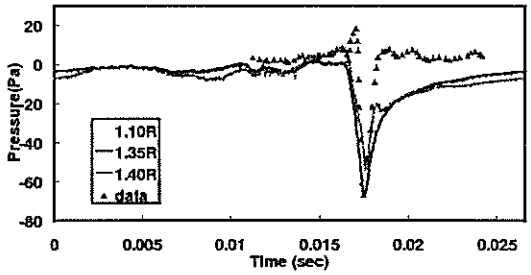

Fig.12 Sensitivity of the Kirchhoff surface on the SPL in the spanwise direction for OLS blade.

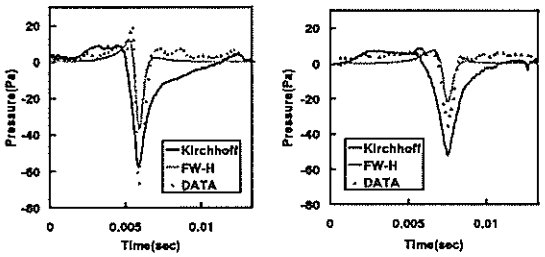

(a) Microphone 2 (b) Microphone 8

Fig.13 Comparison of the noise waveform obtained by Kirchhoff formulation and FW-H formulation for OLS rotor blade.

In the Fig.13, the calculated noise waveforms are compared with the experimental data at microphone position of ② and ⑧. From this figure, the calculated waveform shows worse expansion characteristics compared with experimental data. However the calculated negative peak magnitude shows comparably good correlation with

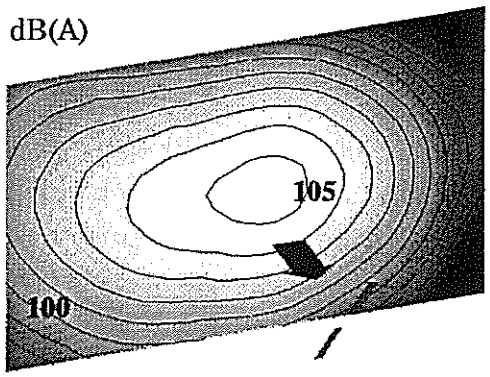

Fig.14 Directivity of the HSI noise at the front plane.

data. This is caused by less accuracy of the calculation. In this figure, the calculated sound pressure waveform used FW-H formulation is also drawn for the comparison with Kirchhoff formulation. The blade pressure is used for the acoustic code of FW-H formulation. As is expected before the calculation, the waveform by FW-H formulation shows under-prediction of the SPL. The missing of the disturbance emitted from the shockwave causes this discrepancy. Fig.14 shows the directivity of the HSI noise. The carpet contour was shown on the perpendicular plane, which is located at the $3.44R$ distance from the rotor center. The highest noise level region is located ahead of the rotor in the rotor rotational plane.

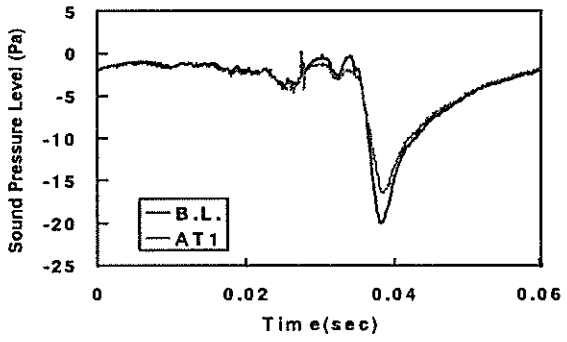

Fig.15 Comparison of the waveform between Baseline and AT1 blade of ATIC

Finally the SPL of AT1 blade was compared with that of the baseline blade in order to validate the low HSI noise characteristics of AT1 blade. AT1 blade was basically designed to reduce the noise by ATIC. Fig.15 shows the calculated waveforms of AT1 and baseline blades. From

this figure, AT1 blade has the lower noise characteristics than that of baseline blade.

4. Conclusions

The predictions of the Helicopter HSI noise are performed using a combined method of a unsteady Euler code with an aeroacoustic code based on the Kirchhoff formulation. Computations are performed for three different blades by using NAL NWT super computer to evaluate capability of this combined method. The following conclusions are drawn.

(1) The combined method (the MOGM with an unsteady Euler code plus the rotating Kirchhoff method) shows reasonable agreement with experiment concerned with the negative peak pressure, however the expansion wave could not be well captured. Further sophisticated treatment in the calculation should be necessary.

(2) The MOGM has considerable potential to capture the precise tip vortex in order to investigate the effect of the interaction between a helicopter rotor and fuselage and /or tail rotor on the noise characteristics.

(3) The present method clearly showed that AT1 blade by ATIC has lower noise characteristics.

(4) The present method needs huge number of computation cost (i.e. CPU time and memory). Therefore more sophisticated computational techniques should be necessary.

5. References:

1.Ffowcs Williams, J.E. et al: Sound Generation by Turbulence and Surface in Arbitrary Motion, Philosophical Trans. of the Royal Society of London, Series A, Vol.264, pp.21-342, 1969.

2.Lighthill, M.J.: On sound Generated Aerodynamically: I. General Theory, Proceedings of the Royal Society of London, Series A: Mathematical and Physical Sciences, Vol.211, No.1107, pp.564-587, 1952.

3.Farassat, F.: Theory of Noise Generation from Moving Bodies with an Application to Helicopter Rotors, NASA TR R-451, 1975.

4.Nakamura, Y., et al: Rotational Noise of Helicopter Rotors, Vertica, Vol.3, No.3/4, pp.293-316, 1979.

5.Boxwell, D.A., et al: Hovering Impulsive Noise: Some Measure and Calculated Results, Vertica, Vol.3, 1979.

6.Hanson, D.B., et al: The Impulsive of Quadrupole sources in Prediction of Transonic Tip Speed Propeller Noise, Journal of Sound and Vibration, Vol.62, No.1, 1979.

7.Schmitz, F.H., et al: Transonic Rotor Noise – Theoretical and Experimental Comparison, Verica, Vol.5, No.2, 1981.

8.Aggarwal, H.R.: The Calculation of Transonic Rotor Noise, AIAA Journal, Vol.22, No.7, 1984.

9.Prieur, J.: Calculation of Transonic Rotor Noise Using Frequency Domain formulation, AIAA Journal, Vol.26, No.2, 1988.

10.Baeder, J.D.: Euler Solution to Nonlinear acoustics of Non-lifting Hovering Rotor Blades, 16th European Rotorcraft Forum, 1990.

11.Isom, M., et al: Geometrical Acoustics and Transonic Helicopter Sound, AIAA paper 87-2748, 1987.

12.Purcell, T.W.: A Prediction of High Speed Rotor Noise, AIAA paper 89-1132, 1989.

13.Pierce, A.D.: Acoustics: An introduction to its Physical Principles and Applications, Mc Graw-Hill, New York, 1981.

14.Zibi, J., et al: Prediction of HSI Noise Using a Coupled Euler/Kirchhoff method for a Helicopter in Hoverflight, 22nd European Rotorcraft Forum, Paper No. 49, 1996.

15.Polacsek, C., et al: High Speed Impulsive Noise computations in Hover and Forward flight Using a Kirchhoff Formulation, 16th AIAA Aeroacoustics Conference, 1995.

16.Strawn, R.C., et al: Computation of Helicopter Rotor Acoustics in Forward Flight, 19th Army Science Conference, 1994.

17.Zibi, J., et al: Helicopter Rotor Noise Predicting Using ONERA and DLR Euler/Kirchhoff Methods, AHS specialists' Meeting for Rotorcraft Acoustics and Aerodynamics, 1997.

18.Aoyama, T., et al: Unsteady Calculation for Flowfield of Helicopter rotor with Various Tip shapes, 18th European rotorcraft forum, 1992.
19.Aoyama, T., et al: Unsteady Analysis of Transonic Helicopter Rotor, 19th European Rotorcraft Forum, 1993.
20.Saito, S. et al: Aeroacoustic Analysis of Transonic Helicopter Rotor Noise, International Pacific Air & space Technology conference, SAE 940041, 1994.
21.Aoyama, T., et al: Blade Planform Design for the Advancing Side of a Helicopter rotor with CFD Technique, 3rd world congress on Computational Mechanics, 1994.
22.Aoyama, T., et al: Effect of Blade Tip Shape on High-speed rotor Noise, AIAA 96-2380, 1996.
23.Zibi, J., et al: Predictions of High-Speed Impulsive Rotor Noise Using Euler/Kirchhoff Methods of ONERA and NAL, AHS International Meeting on Rotorcraft advanced technology and disaster relief, PaperNo.T4-1, 1998.
24.Aoyama, T., et al: Calculation of rotor Blade-vortex Interaction Noise Using Parallel Super computer, 22nd European rotorcraft Forum, 1996.
25.Nishimura, H., et al: Comparison between Calculated Rotor Noise and Experimental Data Obtained DNW Test, 24th European Rotorcraft Forum, 1998.
26.Ochi, A., et al: Parallel Numerical computation of Helicopter Rotor by Moving Overlapped Grid Method, AHS International Meeting on Advanced Technology and Disaster Relief, 1998.
27.Ochi, A., et al: Aerodynamic and Aeroacoustic analysis of BVI by Moving Overlapped Grid Method, 24th European rotorcraft forum, 1998
28.Ochi, A. et al: BVI Noise Prediction by Moving Overlapped Grid Method, 55th AHS Annual Forum and Technology display, 1999.
29.Yamamoto, S., et al: Journal of Computers & Fluids, Vol.22, pp.259-270, 1993.
30.Shima, E., et al: Role of CFD in Aeronautical Engineering (No.14) –AUSM type Upwind Scheme-, NAL SP-34, 1996.
31.Ochi, A., et al: A Numerical Simulation of Flow around Rotor Blades Using Overlapped Grid, NAL SP-37, 1997.
32.Farrasat, F., et al: Extension of Kirchhoff's Formula to Radiation from Moving surfaces, Journal of Sound and Vibration, Vol.123, No.3., pp.451-461, 1988.
33.Farassat, F.,: Discontinuities in Aerodynamics and aeroacoustics: The concept and Applications of Generalized Derivatives, Journal of Sound and Vibrations, Vol.55, No.2, 1977.
34.Boxwell, D.A., et al: Model Helicopter Rotor High-Speed Impulsive Noise: Measured Acoustics and Blade Pressures, NASA TM 85850, 1983.